Proc. SPIE, Vol.8554 (2012) 85541G-1~85541G-9 (9 pages)

Optimization of the experimental parameters of cesium CPT system

Zhi LIU, Jieying WANG, Wenting DIAO, Jun HE, and Junmin WANG*

State Key Laboratory of Quantum Optics and Quantum Optics Devices (Shanxi University),
and Institute of Opto-Electronics, Shanxi University
No.92 Wu Cheng Road, Taiyuan 030006, Shanxi Province, P. R. China

ABSTRACT

Based on a Λ-type three-level system consists of cesium (Cs) $6S_{1/2}$ (Fg = 3) and $6S_{1/2}$ (Fg = 4) long-lived ground states and $6P_{3/2}$ (Fe = 4) excited state, we have experimentally measured and theoretically analyzed the characters of coherent population trapping (CPT) resonances in Cs vapor cells with different partial pressure of neon (Ne) as buffer gas around room temperature. The impact of some experimental parameters, such as the relative intensity ratio between two phase-locked laser beams, the laser intensity, with or without buffer gas and the partial pressure of Ne, the temperature and the longitudinal magnetic field, on the CPT resonance was studied in details. With the optimized parameters, we got typical CPT signal with the full-width half-maximum (FWHM) linewidth as narrow as ~ 181 Hz in a Cs vapor cell filled with 30 Torr of Ne as buffer gas.

Keywords: Coherent population trapping (CPT), linewidth, signal amplitude, phase locking of large-frequency-difference lasers, cesium (Cs) atoms, buffer gas, magnetic shielding

1. INTRODUCTION

Two phase-locked laser fields which match the hyperfine splitting of ground state of alkali metal atoms lead the Λ-type three-level atoms to be driven in a superposition dark state and photons are not absorbed anymore. This has been called coherent population trapping (CPT) effect. It was first observed in1976 by Alzetta *et al* [1]. Then CPT effect has been proposed for applications in the field of atom cooling [2], high-sensitivity magnetometer [3] and atomic clock [4-5].

In the case of alkali metal atoms, the two phase-locked laser fields are applied to couple the Λ-type three-level atoms with the two hyperfine levels of the $S_{1/2}$ ground state and one hyperfine level of the $P_{1/2}$ or $P_{3/2}$ excited state. Atomic coherence is created in the ground state. When CPT occurs, atoms are prepared in a superposition dark state, actually no atoms are excited to the $P_{1/2}$ or $P_{3/2}$ excited state, we can either observe a narrow dark line in the fluorescence spectra or a narrow increased transmission peak [6]. The CPT signal's linewidth $\Delta\upsilon$ is limited by the decoherence time τ of the superposition dark state in ground state ($\Delta\upsilon \propto 1/\tau$). Normally the ground-state coherence can have an extremely long decoherence lifetime, especially when some techniques for protecting atomic coherence, for example, proper buffer gas or paraffin coating in atomic vapor cell, are adopted. This yields much narrower CPT linewidth (several hundred Hz or below), and will improve the frequency stability of atomic clock.

In this paper, based on a Λ-type three-level system consists of cesium (Cs) $6S_{1/2}$ (Fg = 3) and $6S_{1/2}$ (Fg = 4) long-lived ground states and $6P_{3/2}$ (Fe = 4) excited state, we have experimentally measured and theoretically analyzed the characters of CPT resonances in Cs vapor cells with different partial pressure of neon (Ne) as buffer gas around room temperature. Employing advantage of our laser system in which the parameters can be arbitrarily changed, in particular, the relative intensity ratio of two phase-locked laser beams can be arbitrarily adjusted, the impact of some experimental parameters, such as the relative intensity ratio between two phase-locked laser beams, the laser intensity, with or without buffer gas and the partial pressure of Ne, the temperature and the longitudinal magnetic field, on the CPT resonance was studied in details.

2. EXPERIMENTAL SETUP OF THE PHASE-LOCKED LASERS WITH A LARGE FREQUENCY DIFFERENCE AND THE CPT MEASUREMENT

The experimental setup consists of a home-made 852-nm extended-cavity diode laser (ECDL) as master laser (ML), and a single-mode 9-mm-can-packaged Fabry-Perot-type GaAlAs semiconductor laser (JDSU 5411-G1) as slave laser (SL), see Fig. 1. The typical ML output power is ~ 60 mW with a linewidth of ~500 kHz (in 50 ms), and SL output power is ~ 100 mW. Using saturation absorption technique, we lock the ML's frequency to the Cs Fg = 3 - Fe = 4 hyperfine

* Email: wwjjmm@sxu.edu.cn (corresponding author)

Quantum and Nonlinear Optics II, edited by Qihuang Gong, Guang-Can Guo,
Yuen-Ron Shen, Proc. of SPIE Vol. 8554, 85541G · © 2012 SPIE
CCC code: 0277-786/12/$18 · doi: 10.1117/12.999897

transition. The ~ 9.193 GHz radio frequency (RF) modulation signal is applied directly on SL's laser head by a bias-T (Picosecond Pulse Labs, model 5547) with a low-phase-noise RF function generator (Agilent 8257C). Typical positive (or negative) first-order modulation sideband is 1~2% of SL's output power when the ~ 9.193 GHz RF power is +17 dBm. A part of ML's output beam is injected into SL's positive first-order sideband for optical injection locking. At this time, the SL's carrier just work at the Cs Fg = 4 – Fe = 4 hyperfine transition (Fig. 2(a)), and the frequency deviation from ML is ~ 9.193 GHz. The RF frequency can be easily scanned around 9.193 GHz, but the injection locking can be maintained [7]. In order to verify the phase coherence of ML and the SL's carrier, we performed beat-note measurement by using of a fast photodiode and a RF spectrum analyzer (Agilent E4405B) [7]. A part of ML's output is shifted +100 MHz by an acousto-optical modulator (AOM), in order to distinguish the beat-note signal. The beat-note signal is shown in Fig. 2(b) with center frequency of 9.293 GHz (9.193 GHz + 100 MHz). The relative linewidth between ML and the SL's carrier is ~ 1.02 Hz which means that the phase between ML and the SL's carrier has been locked with a frequency difference of 9.193 GHz.

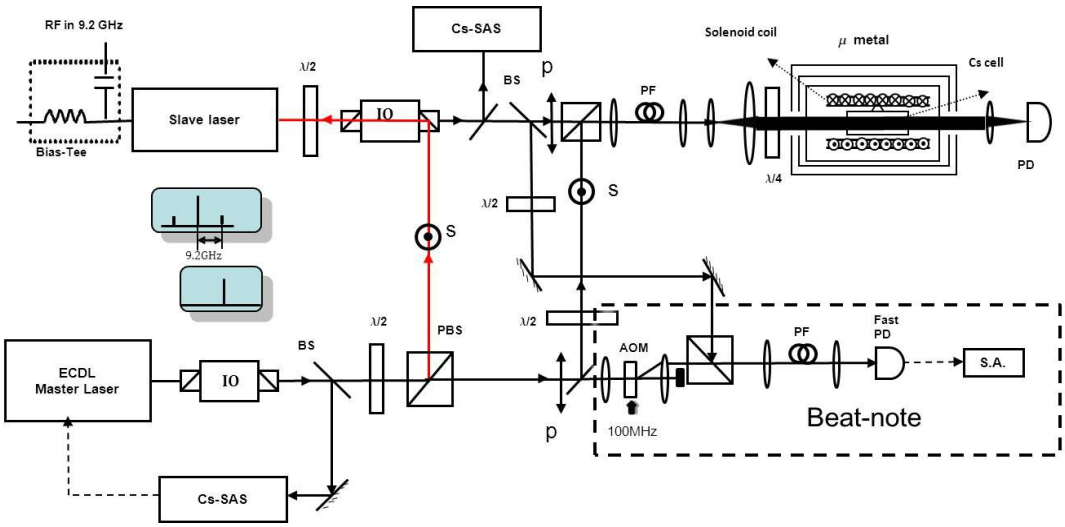

Fig. 1 Experimental setup used to observe narrow coherent population trapping resonances and beat-note signal. ECDL: extended-cavity diode laser, IO: optical isolator, Cs-SAS: Cs saturation spectroscopy, BS: beam splitter plate, PBS: polarizing beam splitter, λ/2: half-wave plate, λ/4: quarter-wave plate, S: s-polarization, P: p-polarization, PD: photodiode, S.A.: RF spectrum analyzer (Agilent E4405B).

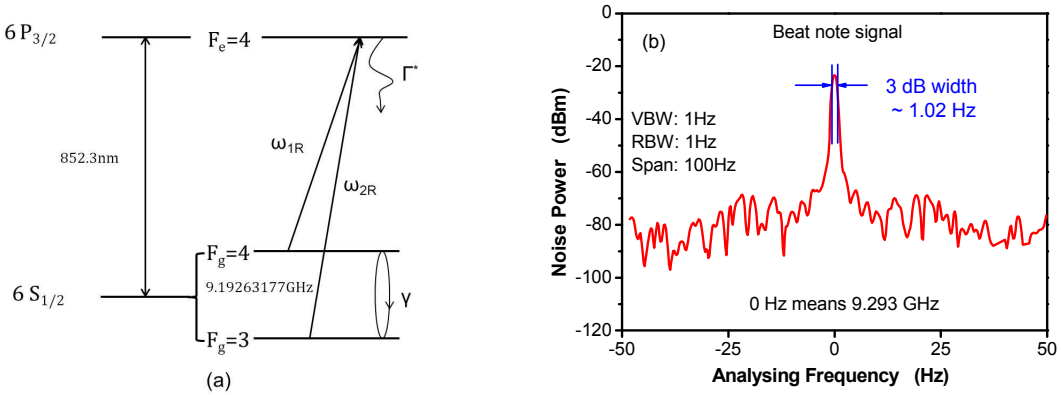

Fig. 2(a) The Λ-type three-level system consists of Cs $6S_{1/2}$ (Fg = 3) and $6S_{1/2}$ (Fg = 4) long-lived ground states and $6P_{3/2}$ (Fe = 4) excited state. Two phase-locked laser beams, ω_{1R} and ω_{2R}, with a frequency difference which equals to the hyperfine splitting of Cs ground state (9.19263177 GHz) couple Fg = 4 – Fe = 4 and Fg =3 – Fe = 4 hyperfine transitions, respectively. (b) Beat-note signal between ML and the SL's carrier. The RF spectrum analyzer's video bandwidth (VBW) and resolution bandwidth (RBW) are set to 1 Hz. The relative linewidth is ~ 1.02 Hz.

The laser beams are superposed on a polarization beam splitter (PBS) cube, and then passed through a single-mode polarization-maintaining (PM) fiber in order to have clean and perfectly overlapped Gaussian profiles. Both beams are circularly polarized by a λ/4 wave plate and then pass through Cs vapor cell (with or without Ne as buffer gas). The Cs vapor cell is placed inside a three-layer μ-metal magnetic shielding tank with typical minimum residual filed of ~ 1 nT. The Cs vapor cell can be heated and temperature stabilized by a temperature controller with a NTC thermistor as sensor and twisted-pair constantan wires as heater (in order to avoid creating addition magnetic field) inside the magnetic shielding tank. Also a solenoid around the Cs cell is mounted inside the tank to set a proper longitudinal magnetic field. The transmitted signal is detected on a photodiode.

3. EXPERIMENTAL RESULTS AND DISCUSSIONS

Based on the Λ-type three level system, the full-width half-maximum (FWHM) linewidth Δυ and amplitude S of CPT signal can be expressed as following [4]:

$$\Delta\upsilon = \frac{1}{\pi}\left(\gamma + \frac{\omega_{1R}^2 + \omega_{2R}^2}{2\Gamma^*}\right), \tag{1}$$

$$S \propto \frac{\omega_{1R}^2 \omega_{2R}^2}{\Gamma^*} \cdot \frac{1}{\gamma + \frac{\omega_{1R}^2 + \omega_{2R}^2}{2\Gamma^*}}, \tag{2}$$

Here Rabi angular frequency ω_{1R} and ω_{2R} are determined by laser intensity, $\omega_R = 2\pi \cdot \Gamma^* \sqrt{I / 2I_s}$. Γ^* is the total decay rate from the excited state Fe = 4 to the two ground levels Fg = 3 and Fg = 4 (affected by spontaneous emission, collide between atoms and buffer gas). Coherence in the ground state tends to zero at the rate γ (affected by collisions between atoms and buffer gas). Resonance strength S depends on atomic population in the superposition dark state.

Two phase-locked laser beams are expanded to a $1/e^2$ radius of ~ 7.9 mm by using a telescope, and then pass through the Cs cell which is placed in the magnetic shielding tank at room temperature. In our experiment, we used several different Cs cell with the same dimensions (ϕ 25 mm x 75 mm, one pure Cs vapor cell, and four cells filled with 2, 10, 20, 30 Torr each of Ne as buffer gas). Fig. 3 shows typical CPT signal with a Cs vapor cell filled with 30 Torr of Ne as buffer gas. The FWHM linewidth is ~181 Hz. The laser intensity of each two incident beam (I_{ML} and I_{SL}) is ~2.5 μW/cm^2.

We are inspired from the pioneer work described in ref [4] and have characterized CPT resonances with varied experimental parameters, such as the relative intensity ratio between two phase-locked laser beams, the laser intensity, with or without buffer gas and the partial pressure of Ne, the magnetic field, and the temperature of Cs cell. We have also made some qualitative analysis based on eq. (1) and (2) and our experimental results.

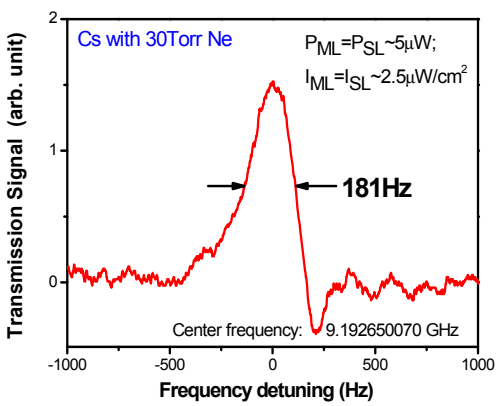

Fig. 3 Typical CPT signal with a Cs vapor cell filled with 30 Torr of Ne as buffer gas. The FWHM linewidth of the CPT signal is ~ 181 Hz.

3.1 Relative intensity ratio between two phase-locked laser beams

Compared to the ± 1-order sidebands generated by direct-current-RF-modulated vertical-cavity surface-emitting laser (VCSEL) [8-10] as phase-locked components, using the technique in which optical injection-locking to the +1 or -1 order of the RF-modulated slave laser by the master laser can easily change the optical intensity of each two phase-locked laser beams, but of course the laser system is little bit complicated (this point is bad for practical using, but is good for basic research). We changed the relative intensity ratio between the two phase-locked laser beams in the case of keeping the total power constant at ~ 60 μW/cm^2. The results are shown in Fig. 4. The relative intensity ratio closes to (I_{ML}/I_{SL}: 1.0~1.4), yields much narrower FWHM linewidth of CPT signal. When the ratio is far from 1, most atoms are optially pumped to one of the hyperfine level of ground states, causing an obvious increase in CPT linewidth and decrease in amplitude [9].

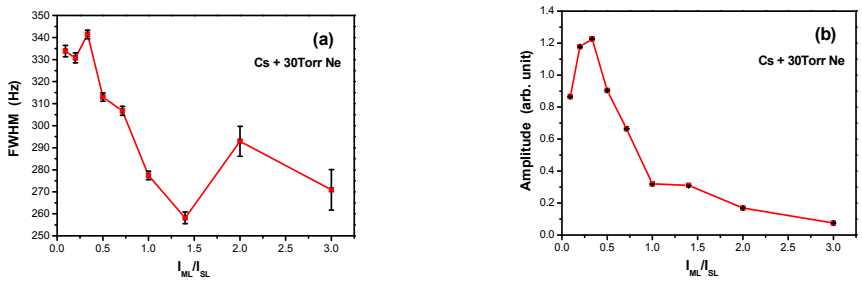

Fig. 4 The FWHM linewidth of CPT signal as a function of relative intensity ratio between coherent bi-chromatic light fields at room temperature.

3.2 Laser intensity and buffer gas

The CPT resonance's shape and linewidth versus the total light intensity were investigated in ref [11-13]. We measured the FWHM linewidth and amplitude of CPT signal versus the light intensity for five different Cs–Ne cells. The results are shown in Fig. 5(a)-(d).

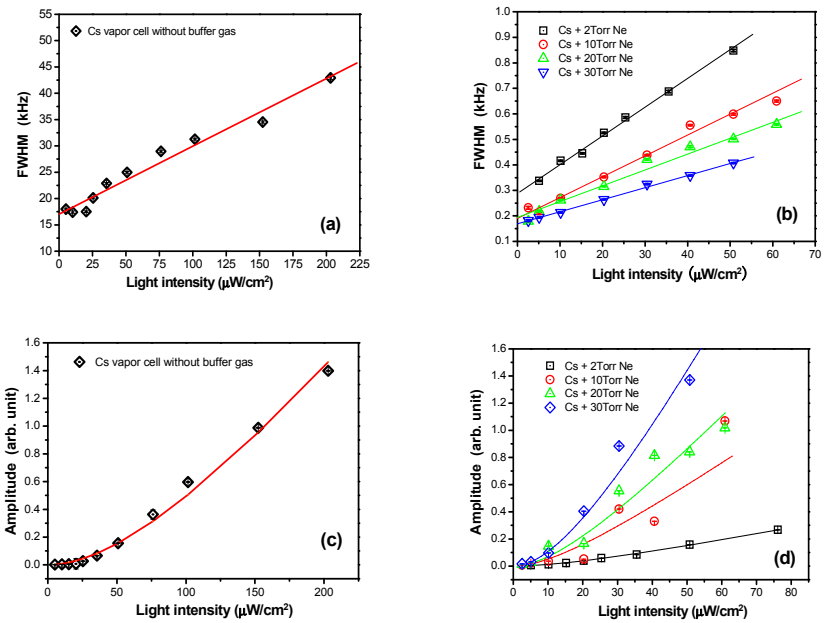

Fig. 5 The FWHM linewidth and amplitude of CPT signal as a function of laser intensity at room temperature. (a)(c) Pure Cs cell. (b)(d) Four Cs-Ne cells with different partial pressure of Ne. The points are measured data, while the solid lines are theoretical fitting according to Eqs. (1) and (2). The laser intensity of each two coherent light is equal, Cs vapor cell placed in the magnetic shielding tank with residual magnetic field of ~ 1 nT.

At first, the results of Fig. 5 (a) and (b) confirm that the FWHM linewidth of CPT signal is linearly dependent on the light intensity [12-15]. According to formula (1) and (2), Rabi angular frequency are substituted by $\omega_R = 2\pi \cdot \Gamma^* \sqrt{I / 2I_s}$, and $I_{ML}=I_{SL}=I$, we have:

$$\Delta\upsilon = \frac{1}{\pi}(\gamma + \frac{2\pi^2 \cdot \Gamma^* \cdot I}{I_s}) \tag{3}$$

$$S \propto \frac{4\pi^4 \cdot \Gamma^{*3} \cdot I^2}{I_s^2} \cdot \frac{1}{\gamma + \frac{2\pi^2 \cdot \Gamma^* \cdot I}{I_s}} \tag{4}$$

For any one of the selected Cs vapor cell, it can be seen that the decay rate Γ^* and the saturation intensity I_s are constants, only the laser intensity is variable. The FWHM linewidth increases linearly with laser intensity due to power broadening, as it formulated in eq. (3). The increasing rate is reflected by the slope which affected by the partial pressure of the buffer gas.

Table 1. Estimated characteristics of Cs–Ne cells at room temperature according to Fig. 4(a) and (b). The size of Cs cell is ϕ25 mm x 75 mm.

Ne Pressure (Torr)	Linewidth γ/π at zero intensity (Hz)	Slope [Hz/(μW/cm^2)]	Relaxation rate γ (Hz)	Decoherence time τ (ms)
0	17000	122.2	53407.1	0.02
2	290.3	11.3	912.0	1.10
10	186.4	8.3	585.6	1.71
20	194.9	6.2	612.3	1.63
30	169.5	4.7	532.5	1.88

In the case of weak intensity, the coherence relaxation rate γ dominantly affects the CPT linewidth. From the CPT linewidth extrapolating to zero intensity from Fig. 5(a) and (b), it is possible to estimate the relaxation rate γ and the decoherence time of any vapor cell (Table.1). It can be seen the variation of the buffer gas' pressure caused the change of γ [12-15].

$$\gamma = \left\{(2.4/a)^2 + (\pi/l)^2\right\} D_0 (P_0/P) + L_0 \cdot \overline{\nu}_{rbg} \cdot g \cdot \sigma_{2bg} (P/P_0) + \gamma_{se} \tag{5}$$

Where D_0 is the diffusion constant in the cylindrical Cs atomic vapor cell with a length l and a diameter a, containing buffer gas with a partial pressure P, P_0 is one atmosphere, L_0 corresponds to the Loschmidt constant, $\overline{\nu}_{rbg}$ is the average relative velocity of Cs atoms and the buffer gas atoms, σ_{2bg} is the Cs–buffer gas collision cross section, and γ_{se} is the coherence spin exchange relaxation rate. First term in the right side represents Cs atoms diffuse to the walls of the cell in the buffer gas, and it decreases with increasing P. The second term in the right side represents the collision of Cs atoms and the buffer gas atoms, and it increases with increasing P. At moderate pressures, the first term plays a major role, the buffer gas will reduce Cs atoms' diffusion to the cell wall. And at high pressures, the Cs–buffer gas (the second term) collision dominate the coherence relaxation rate. At high temperatures, the third term makes spin exchange relaxation predominant (high Cs atomic density). As the temperature increases, the mean relative speed of Cs atoms increases, and γ_{se} increases too.

For our Cs-Ne vapor cells in the moderate pressure, γ is mainly decided by the first item, the buffer gas reduced transit time broadening. At the same time, Cs–buffer gas collision reduced the rate of Cs atoms' diffusion and Cs-cell wall collision, the relaxation rate γ of the two hyperfine levels in Cs ground state declined. Therefore, the FWHM linewidth of CPT signals reduced (Fig. 6(a)), the amplitude increased (Fig. 6(b)). The results are in good agreements with eqs. (3) and (4) qualitatively.

Although the buffer gas can reduce the FWHM linewidth of CPT signal effectively, but at the same time it has brought the shift of the center frequency of CPT resonance [11]. In Fig. 7 the CPT frequency shift is plotted as a function of

the partial pressure of Ne buffer gas at room temperature. A linear fitting gives a frequency shift rate of ~570 Hz/Torr. Therefore, optimizing the partial pressure ratio of the two kind buffer gases which have opposite frequency shift factor (Ar-Ne or CH_4-N_2) can minimize or eliminate the frequency shift. And it will reduce the temperature sensitivity of the CPT resonance frequency [16]. Above-mentioned experimental results and discussions will be helpful for improving the frequency stability of CPT atomic clock.

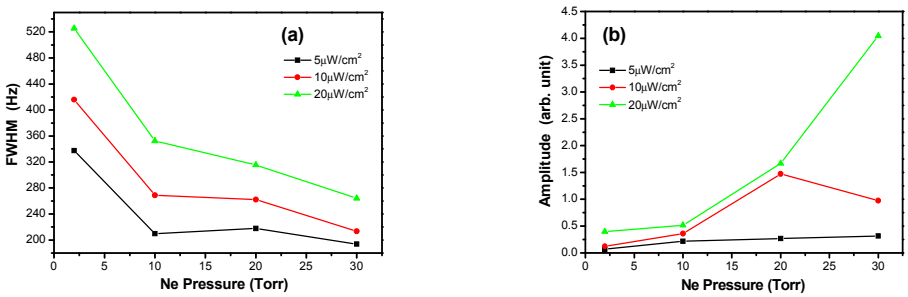

Fig. 6 The FWHM linewidth of CPT signal as a function of Ne pressure at room temperature

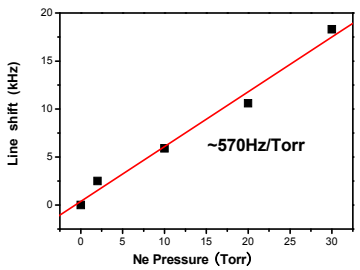

Fig. 7 Frequency shift of CPT resonance line as a function of Ne partial pressure at room temperature.

3.3 Magnetic field

Because of the complex magnetic environment in our laboratory, angle between the net magnetic field direction and laser propagation direction is uncertain. Shielding the stray magnetic field, we can clearly see the impact of the magnetic field on the CPT resonance. We placed the pure Cs cell inside the magnetic shielding tank with residual magnetic field of ~ 1 nT, and a uniform magnetic field is applied in the longitudinal direction (the direction of laser propagation) via a solenoid. We observed that the FWHM linewidth of CPT signals linearly increased when the longitudinal magnetic field increased (Fig. 8). This point is in consistent with ref [17]. With increasing of the longitudinal magnetic field, see Fig. 9(b), yielding the Zeeman sublevels' frequency shift increases ($\Delta\nu = g_F \mu_B B/\hbar$, for the ground state of the Cs atom, $\Delta\nu/\Delta B$ = - 3.5 kHz/μT for Fg = 3 level, $\Delta\nu/\Delta B$ =3.5 kHz/μT for Fg = 4 level). So the FWHM linewidth of CPT signal will be broaden.

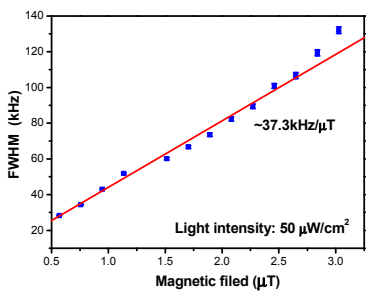

Fig. 8 The FWHM linewidth of CPT signal as a function of the longitudinal magnetic field.

The FWHM linewidth of CPT signal without the applied longitudinal magnetic field is ~31.1 kHz. When we continue to increase the longitudinal magnetic field to B ~ 6.8 μT, CPT transmission signal splits into seven peaks, as shown Fig. 9(a). This result is consistent with the experimental observation in ref [18] and the theoretical model with $\sigma^- - \sigma^-$ polarizations of the two phase-locked laser beams in ref ref [19]. Frequency span between the first peak and the seventh peak is ~ 284.7 kHz, and it is close to theoretically calculated value (12 x B x ($\Delta\nu/\Delta B$ = 3.5 kHz/μT) ~285.6 kHz). The FWHM linewidth for the middle CPT component for the Λ-type three-level system consists of |Fg = 3, m_F = 0>, |Fg = 4, m_F = 0> and |Fe = 4, m_F = 0> states is ~18.9 kHz.

This splitting can be understood in the schematic diagram shown in Fig. 9(b). When the two phase-locked laser beams with$\sigma^- - \sigma^-$ circular polarizations and with the moderate longitudinal magnetic field, clearly 7 sets of Λ-type three-level sub-system will separate in frequency domain. Under the condition of weak magnetic field, the seven CPT peaks due to seven sets of Λ-type three-level sub-system are partially superposed, yields one broadened CPT transmission peak. This is the main physics behind Fig. 8. With the increase of the longitudinal magnetic field to certain value, the FWHM linewidth of CPT signal increases gradually until splits into seven peaks. The magnetic filed intensity can be derived from measuring the frequency splitting. This is the basic principle of the CPT magnetometer.

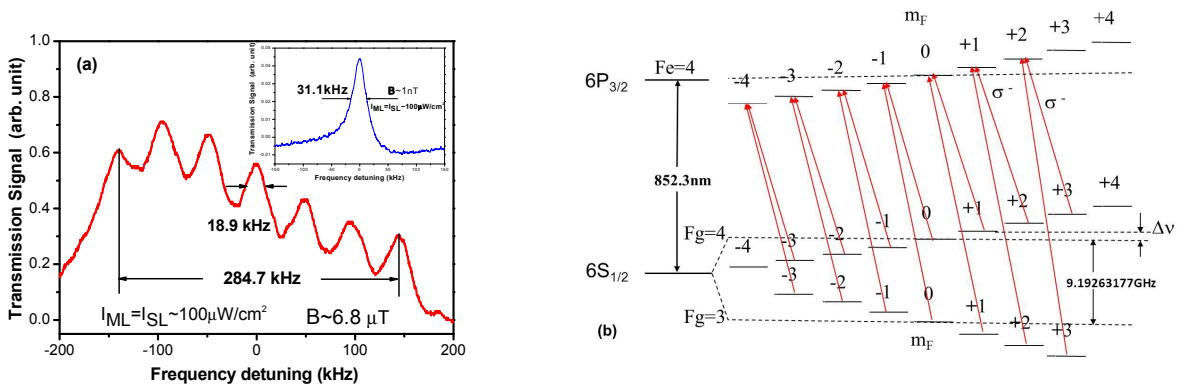

Fig. 9 (a) When the longitudinal magnetic field in the Cs cell region increases to certain value, the CPT transmission splits into several peaks due to Zeeman effect. Typical parameters: pure Cs vapor cell, optical intensity of each two phase-locked laser beams ~100 μW/cm^2, ~ 6.8 μT of the longitudinal magnetic field. The inset is a typical CPT resonance transmission signal under the same conditions but without longitudinal magnetic field. (b) Schematic diagram of nonzero magnetic field environment for with the two phase-locked laser beams with $\sigma^- - \sigma^-$ circular polarizations. Zeeman effect induces splitting of the Zeeman sublevels. Clearly seven sets of Λ-type three-level system are separated in frequency domain.

3.4 Cell temperature

A series of CPT signals are measured for various temperatures of the Cs cell filled with 20 Torr of Ne as buffer gas (Fig. 10). In this set experiment, the CPT linewidth slightly decreases with the cell temperature until ~ 35 °C where it seems to rise again. The increase in temperature also causes the atomic vapor to become optically thick because of the increase in the absorption coefficient α. The CPT linewidth decreases slightly because of a reduction in the laser intensity along the cell path. For the absorbed fraction it follows that [20]:

$$1-\frac{I_{\text{trans}}(\text{L})}{I_0}=1-\exp[-\alpha(\text{T})\cdot\text{L}]=1-\exp[\frac{-\upsilon_{abs}}{T}\exp(-\frac{T_0}{T})] \tag{6}$$

Where L is the length of the atomic vapor cell. Obviously, the higher the temperature T, the absorption rate is closer to 1. The linewidth of CPT signal should be a function of the laser intensity at every position in the light path over the whole cell, and it depends on the intensity of the transmitted laser beam (Section 3.2 of this article confirm this point). Therefore, the CPT linewidth decreases with increasing temperature at first. Simultaneously, according to eq. (5), the last term represents the contribution to the ground state coherence of the Cs–Cs spin-exchange collisions. It is given by [4]

$$\gamma_{\text{se}}=\frac{6I+1}{8I+4}\cdot\overline{\upsilon}_r\cdot n_{cs}\cdot\sigma_{se} \tag{7}$$

Where I = 7/2 is Cs nuclear spin, σ_{se}=2.18×10^{-14} cm^2 is Cs spin exchange cross section, n_{cs} is the Cs atomic density, $\overline{\upsilon_r}=\sqrt{(8k_BT)/(\pi\mu_{cs})}$ is the average relative speed of Cs atoms, k_B = 1.38×10^{-23} J/K is the Boltzmann constant, and μ_{cs} is the Cs reduced mass. The CPT linewidth broadening due to Cs–Cs spin-exchange collisions is increased when the cell temperature > 35 °C for 75-mm-long Cs vapor cell. At high temperatures, according to eq. (7), the higher Cs atomic density makes spin-exchange relaxation predominant. As the temperature increases, the average relative speed of Cs atoms increases, so γ_{se} increases, and the CPT linewidth will be broaden.

The amplitude reaches its maximum value when the cell temperature < 25 °C, and then it drops rapidly with higher temperatures, further it disappears completely when the cell temperature >40 °C, because the 75-mm-long Cs vapor cell contains enough Cs atoms even at room temperature. We note that the amplitude of the resonance is proportional to the number of Cs atoms in the superposition dark state. As the number of Cs atoms in the vapor cell increases further, more photons are absorbed by those atoms not in the superposition dark state. At temperature near 40 °C, atomic vapor in the cell becomes very dense, thus almost no resonant light can pass through the cell. If using a shorter atomic vapor cell, the temperature for the maximum ratio of CPT amplitude over linewidth will shift to a higher temperature [13, 15, 20].

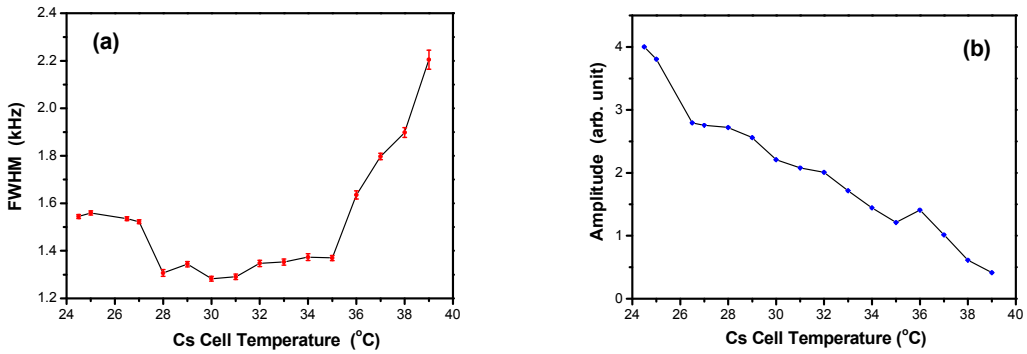

Fig. 10 The FWHM linewidth and amplitude of CPT signals of Cs cell filled with 20 Torr of Ne as buffer gas versus cell temperatures. The laser intensity of each two phase-locked laser beams is ~150 μW/cm^2. Cs cell is placed in the magnetic shielding tank with a residual field of ~ 1 nT.

4. CONCLUSIONS

We have studied the impact of some experimental parameters, such as relative intensity ratio between two phase-coherent laser beams, laser intensity, buffer gas, cell temperature and longitudinal magnetic field, on the CPT resonance in details. Results show that ratio of the light close to 1, weak laser intensity, the suitable partial pressure of the buffer gas (Ne) and good magnetic shielding are very helpful to get a further narrowed FWHM linewidth of the CPT signal. Finally, under the optimized parameters, we get typical CPT signal's FWHM linewidth as narrow as ~181 Hz.

ACKNOWLEDGMENT

This work was supported by the National Natural Science Foundation of China (Grant Nos. 60978017, 61078051, 11274213 and 61205215), the National Major Scientific Research Program of China (Grant No. 2012CB921601), the Research Project for Returned Abroad Scholars from Universities of Shanxi Province, China (Grant No. 2012-015) and the Project for Excellent Research Team of the National Natural Science Foundation of China (Grant No. 61121064).

REFERENCES

[1] Alzetta G, Gozzini A, Moi L and Orriols G, "An experimental method for the observation of rf transitions and laser beat resonances in oriented Na vapor", Nuovo Cimento B 36, 5 (1976).

[2] Aspect A, Arimondo E, Kaiser R, Vansteenkiste N and Cohen-Tannoudji C, "Laser cooling below the one-photon recoil energy by velocity-selective coherent population trapping", Phys. Rev. Lett. 61, 826 (1988).

[3] Scully M O and Fleischauer M, "High-sensitivity magnetometer based on index-enhanced media", Phys. Rev. Lett. 69, 1360 (1992).
[4] Vanier J, Godone A and Levi F, "Coherent population trapping in cesium: dark lines and coherent microwave emission", Phys. Rev. A 58, 2345 (1998).
[5] Knappe S, Shah V, Schwindt P D D, Hollberg L, Kitching J, Liew Li-Anne and Moreland J, "A micro-fabricated atomic clock", Appl. Phys. Lett. 85, 1460 (2004).
[6] Vanier J, "Atomic clocks based on coherent population trapping: a review", Appl. Phys. B 81, 421 (2005).
[7] Diao W T, He J, Liu Z, Yang B D and Wang J M, "Alternative laser system for cesium magneto-optical trap via optical injection locking to sideband of a 9-GHz current-modulated diode laser", Opt. Express 20, 7480 (2012).
[8] Liu G B, Zhao F and Gu S H, "Study of a low power dissipation, miniature laser-pumped rubidium frequency standard", Chinese Phys. B 18, 3839 (2009).
[9] Wang Z, Deng K, He D W, Liu X Y, Liu L, Guo T and Chen X Z, "Effects of the intensity difference of two laser fields on coherent population trapping clocks", IEEE Int. Freq. Contr. Symp. 7, 669 (2008).
[10] Affolderbach C, Nagel A, Knappe S, Jung C, Wiedenmann D and Wynands R, "Nonlinear spectroscopy with a vertical-cavity surface-emitting laser (VCSEL)", Appl. Phys. B 70, 407 (2000).
[11] Brandt S, Nagel A, Wynands R and Meschede D, "Buffer-gas-induced linewidth reduction of coherent dark resonances to below 50 Hz", Phys. Rev. A 56, 1063 (1997).
[12] Moon H S, Park S E, Park Y H, Lee L and Kim J B, "Passive atomic frequency standard based on coherent population trapping in Rb-87 using injection-locked lasers", J. Opt. Soc. Am. B 23, 2393 (2006).
[13] Boudot R, Dziuban P, Hasegawa M, Chutani R K, Galliou S, Giordano V and Gorecki C, "Coherent population trapping resonances in Cs–Ne vapor microcells for miniature clocks applications", J. Appl. Phys. 109, 014912 (2011).
[14] Wynands R and Nagel A, "Precision spectroscopy with coherent dark states", Appl. Phys. B 68, 1 (1999).
[15] Knappe S, Wynands R, Kitching J, Robinson H G and Hollberg L, "Characterization of coherent population-trapping resonances as atomic frequency references", J. Opt. Soc. Am. B. 18, 1545 (2001).
[16] Deng K, Guo T, He D W, Liu X Y, Liu L, Guo D Z, Chen X Z and Wang Z, "Effect of buffer gas ratios on the relationship between cell temperature and frequency shifts of the coherent population trapping resonance", Appl. Phys. Lett. 92, 211104 (2008).
[17] Zibrov S A, Velichansky V L, Zibrov A S, Taichenachev A V and Yudin V I, "Experimental investigation of the dark pseudo-resonance on the D_1 line of the ^{87}Rb atom excited by a linearly polarized field", JETP Lett. 82, 477 (2005).
[18] Park S E, Kwon T Y and Lee H S, "Production of Raman laser beams using injection-locking technique", IEEE Trans. Instrum. Meas. 52, 277 (2003).
[19] Wynands R, Nagel A, Brandt S, Meschede D and Weis A, "Selection rules and line strengths of Zeeman-split dark resonances", Phys. Rev. A 58, 196 (1998).
[20] Knappe S, Kitching J, Hollberg L and Wynands R, "Temperature dependence of coherent population trapping resonances", Appl. Phys. B 74, 217 (2002).